Role of dispersion on phononic thermal boundary conductance

John C. Duda, Thomas E. Beechem, Justin L. Smoyer, Pamela M. Norris, and Patrick E. Hopkins

Citation: J. Appl. Phys. 108, 073515 (2010); doi: 10.1063/1.3483943
View online: http://dx.doi.org/10.1063/1.3483943
View Table of Contents: http://jap.aip.org/resource/1/JAPIAU/v108/i7
Published by the American Institute of Physics.

Role of dispersion on phononic thermal boundary conductance

John C. Duda,[1,a)] Thomas E. Beechem,[2,b)] Justin L. Smoyer,[1,c)] Pamela M. Norris,[1,d)] and Patrick E. Hopkins[2,e)]
[1]*Department of Mechanical and Aerospace Engineering, University of Virginia, Charlottesville, Virginia 22904, USA*
[2]*Sandia National Laboratories, Albuquerque, New Mexico 87185, USA*

(Received 27 March 2010; accepted 1 August 2010; published online 7 October 2010)

The diffuse mismatch model (DMM) is one of the most widely implemented models for predicting thermal boundary conductance at interfaces where phonons dominate interfacial thermal transport. In the original presentation of the DMM, the materials comprising the interface were described as Debye solids. Such a treatment, while accurate in the low temperature regime for which the model was originally intended, is less accurate at higher temperatures. Here, the DMM is reformulated such that, in place of Debye dispersion, the materials on either side of the interface are described by an isotropic dispersion obtained from exact phonon dispersion diagrams in the [100] crystallographic direction. This reformulated model is applied to three interfaces of interest: Cr–Si, Cu–Ge, and Ge–Si. It is found that Debye dispersion leads to substantially higher predictions of thermal boundary conductance. Additionally, it is shown that optical phonons play a significant role in interfacial thermal transport, a notion not previously explored. Lastly, the role of the assumed dispersion is more broadly explored for Cu–Ge interfaces. The prediction of thermal boundary conductance via the DMM with the assumed isotropic [100] dispersion relationships is compared to predictions with isotropic [111] and exact three-dimensional phonon dispersion relationships. It is found that regardless of the chosen crystallographic direction, the predictions of thermal boundary conductance using isotropic phonon dispersion relationships are within a factor of two of those predictions using an exact three-dimensional phonon dispersion. © *2010 American Institute of Physics*. [doi:10.1063/1.3483943]

I. INTRODUCTION

The continuing miniaturization of today's nanoelectronic devices has introduced more interfaces per unit length for energy carriers to traverse. As a result, the primary thermal resistance in modern devices is the Kapitza, or thermal boundary resistance (R_{BD}), at the various interfaces within these devices. Resistance to thermal transport in solids is due to the scattering of energy carriers as they propagate. The average distance between these scattering events in bulk materials, described by the carrier mean free path (MFP), is on the order of 100 nm at room temperature for phonons,[1] but can vary depending on material and frequency. Abrupt interfaces provide yet another site for carrier scattering. In modern nanostructured devices, with these interfaces spaced at distances smaller than the carrier MFP, scattering is predominantly dictated by boundaries between the materials and not within the materials themselves. In some cases, reduced R_{BD} is desired, while in others, it is not. For example, in transistors, phonon scattering leads to increased self heating and an increase in overall operating temperature, in turn reducing speed and lifetime.[2] On the contrary, in thermoelectric devices, increased phonon scattering reduces effective thermal conductivity, leading to a greater overall figure of merit.[3] Regardless, accurate predictive models are, again, increasingly valuable.

Two models have been most widely employed for predicting R_{BD} at interfaces between different materials: the acoustic mismatch model (AMM) and the diffuse mismatch model (DMM). The AMM treats phonons as waves propagating in a continuous medium and assumes these waves do not scatter at an interface between two different materials; rather, phonon transmission and reflection is controlled by the relative mismatch in acoustic impedance of the materials.[4] Due to this continuum analysis, the AMM works best at low temperatures where dominant phonon wavelengths are long and frequencies are low. The DMM, on the other hand, operates at the other extreme, assuming *all* phonons scatter at the interface and do so diffusely. That is, phonons lose memory of their incident polarization and direction after scattering at the interface.[5] As a result, the DMM holds for elevated temperatures relative to the AMM, but still in a regime where the temperature is much less than the Debye temperature of the materials comprising the interface. Still, the overall accuracy of the DMM has more recently come into question as the model has been applied to a larger regime than that for which it was originally developed.[5] Several studies[6,7] have shown that the agreement between the DMM and experimentally measured values of R_{BD} can vary by up to an order of magnitude.

The DMM is accurate in both form and function in the temperature regime for which it was derived and first ap-

[a)]Electronic mail: duda@virginia.edu.
[b)]Electronic mail: tebeech@sandia.gov.
[c)]Electronic mail: jls5ra@virginia.edu.
[d)]Electronic mail: pamela@virginia.edu.
[e)]Electronic mail: pehopki@sandia.gov.

plied. However, in many subsequent applications, specifically those at elevated temperatures, the DMM does not capture the entire physical picture associated with phonon thermal transport across an interface. Consequently, it suffers from several deficiencies. These deficiencies include (i) a lack of consideration given to the quality and conditions of the interface itself,[8,9] (ii) an inaccurate account of the phonon flux approaching and transmitting across the interface,[10–12] and (iii) an over-simplified description of the materials comprising the interface.[13–15] In many cases, these deficiencies have been addressed at some level, thus increasing one's ability to match predictions to experimental data by eliminating much of the previously discussed error associated with the model.[6,7] A summary of this work is given in the sections below.

A. Quality and condition of the interface

It has been shown that significant interatomic diffusion and roughness at the boundary results in less thermally conductive interfaces.[16] This increase in R_{BD} has been attributed to increased phonon scattering events at a disordered interface. In order to account for interfacial roughness, Beechem *et al.*[8] implemented a virtual-crystal approach (VCDMM), treating the interface between Cr and Si as not one, but two interfaces. The first interface was that between Cr and a Cr–Si alloy, and the second between a Cr–Si alloy and Si. The properties of the Cr–Si virtual crystal were determined through mixing rules based on the composition profiles seen during Auger electron spectroscopy depth profiling.[17] This model was further refined by Beechem and Hopkins in the δ-DMM, treating the interfacial region not as a crystal as is the case in the VCDMM, but instead as an amorphous region, thus more accurately reflecting the true characteristics of the interface.[9] Both the VCDMM and δ-DMM showed considerable improvement in the ability to match predictions to experimental data as compared to the original formulation of the DMM.

B. Phonon flux approaching and transmitting across an interface

In the original formulation of the DMM, it was assumed that phonons scatter elastically at the interface. That is, a phonon with energy $\hbar\omega$ in material A approaching the interface from side 1 can only scatter with a phonon of the same frequency (and hence, energy) in material B on side 2. However, Swartz and Pohl[5] over-enforced this condition by maintaining that the maximum phonon frequency that can participate in interfacial transport was the maximum phonon frequency of the most vibrationally restrictive phonon branch (i.e., the transverse acoustic branch). Duda *et al.*[10] demonstrated that this formulation ignores phonon flux approaching the interface from side 1 that could scatter elastically with phonons on side 2 of the interface. It was shown that, through consideration of this previously ignored flux, the agreement between the DMM and experimental data was drastically improved. In addition, the case for inelastic scattering of phonons at the interface was made by Hopkins and Norris[11] and Hopkins.[12] In both cases, new formulations of the DMM were presented to account for inelastic phonon scattering events at the interface. Each of these approaches showed better agreement between the predicted and experimental data for R_{BD} at interfaces between vibrationally mismatched materials (e.g., the Pb-diamond interface).

C. Describing the properties of the materials comprising the interface

As mentioned above, most formulations of the DMM rely on an isotropic Debye dispersion, and thus, the accuracy of the DMM rests on the ability of an isotropic Debye dispersion to describe the materials comprising the interface of interest. Duda *et al.*[13] extended the applicability of the DMM to interfaces where one material comprising the interface was characterized by extreme elastic and vibrational anisotropy. In doing so, they formulated an effective Debye density of states for graphite, treating the graphite system as a linear assembly of uncoupled two-dimensional systems. Phelan[14] noted that the use of a Debye density of states to describe $YBa_2Cu_3O_{7-\delta}$ (YBCO) thin films resulted in a severe overprediction of R_{BD} at interfaces between YBCO and MgO, where as the use of a measured phonon density of states greatly increased the agreement between the DMM and experimental data. Reddy *et al.*[15] calculated and implemented exact three-dimensional dispersion relationships via the Born-von Karman model (BKM) in the formulation of the DMM when predicting R_{BD} at metal-semiconductor interfaces, noting that the predicted values of R_{BD} differ greatly depending on the assumed dispersion.

D. Present work

The model presented here utilizes pre-existing exact phonon dispersions readily available in the literature to describe the vibrational properties of the two materials comprising the interface. In this sense, no assumptions need to be made regarding the type of dispersion or the form of the phonon density of states, Debye or otherwise. This is particularly beneficial, as Chung *et al.*[18] have demonstrated the impact of assumed dispersion when calculating thermal conductivity. To increase the accessibility of the model while alleviating the otherwise significant computational requirements needed to fully account for the entire three-dimensional dispersion, an isotropic relationship with the characteristics of the [100] crystallographic direction (i.e., the direction perpendicular to the interface) is assumed. The validity of this assumption is evaluated by means of a direct comparison between the present model with the model of Reddy *et al.*[15] for a Cu–Ge interface. All calculations are carried out under both the assumptions of elastic and inelastic scattering, thus establishing lower and upper limits of R_{BD} for three interfaces of interest: Cr–Si, Cu–Ge, and Ge–Si. Unlike with previous formulations of the DMM, optical phonon branches are considered. It is shown that, even in the limit of elastic scattering, these branches can contribute significantly to interfacial transport.[19]

II. PHONON THERMAL TRANSPORT ACROSS AN INTERFACE

The DMM has been derived in full several times in the literature.[5,11,14,20] However, due to the varying assumptions applied during these derivations, many subtleties of the model are confused or even lost altogether.[10] As a result, the authors believe it is important to once again carry out this derivation. Not only will this ensure that these subtleties are not overlooked, but it will become possible to address the relative importance of these subtleties under the present set of assumptions. This being said, the phonon flux, q, across an interface from side 1 to side 2 can be represented as

$$q_z^{1\to 2}=\frac{1}{(2\pi)^3}\sum_j\int_0^{\pi/2}\int_0^{2\pi}\int_{k_{x,1}}\int_{k_{y,1}}\int_{k_{z,1}>0}\hbar\omega_{j,1}(k_{j,1})\zeta^{1\to 2}|v_{j,1}(k_{j,1})|f_0\sin(\theta_1)\cos(\theta_1)dk_{z,1}dk_{y,1}dk_{x,1}d\theta_1 d\phi_1, \tag{1}$$

where z is the direction of transport, j is the polarization, θ_1 and ϕ_1 are the azimuthal and elevation angles of the flux on side 1 approaching side 2 relative to the direction of transport, ζ is the transmission coefficient, v_1 is the carrier group velocity on side 1, f_0 is the equilibrium distribution of particles on side 1, and k is the wave vector. In order to consider only flux approaching the interface, integration is performed over half of the Brillouin zone (BZ) and the absolute value of the group velocity, v_1, is taken. In this present study, the quantity of interest is phonon energy, and thus, the equilibrium distribution, f_0, is given by the Bose–Einstein distribution, $f_0=1/[\exp(\hbar\omega/k_BT)-1]$. Assuming diffuse scattering, the directional dependence of Eq. (1) collapses and the expression for phonon flux across the interface from side 1 to side 2 becomes

$$q_z^{1\to 2}=\frac{1}{8\pi^2}\sum_j\int_{k_{x,j,1}}\int_{k_{y,j,1}}\int_{k_{z,j,1}>0}\hbar\omega_{j,1}(k_{j,1})\zeta^{1\to 2}|v_{j,1}(k_{j,1})|f_0 dk_{z,j,1}dk_{y,j,1}dk_{x,j,1}. \tag{2}$$

This expression can be further simplified by assuming the materials in question can be described by an isotropic phonon dispersion. This yields

$$q_z^{1\to 2}=\frac{1}{8\pi^2}\sum_j\int_{k_{j,1}>0}\hbar\omega_{j,1}(k_{j,1})k_{j,1}^2\zeta^{1\to 2}|v_{j,1}(k_{j,1})|f_0 dk_{j,1}. \tag{3}$$

To validate the assumption of diffuse scattering, we have plotted the specularity parameter, p, as a function of temperature, T, for several different phonon group velocities in Fig. 1. The specularity parameter is a measure of the probability a phonon will scatter specularly at an interface. It is given as $p=\exp[-16\pi^3\delta^2/L^2]$, where δ is the roughness of the interface and L is the phonon coherence length, given as $L=hv/k_BT$.[1] Assuming an interface roughness of 1 nm, the fastest traveling phonons in Si ($v_{max}=8,192$ m/s) have less than a 1% chance of scattering specularly at 40 K. For lower group velocities, rougher surfaces, or higher temperatures, the probability of phonons scattering specularly is even lower. The assumed roughness of 1 nm corresponds to a deviation of ±2 atomic layers at a Cr–Si interface. While near-perfect interfaces (roughness near one atomic layer) can be achieved through epitaxial growth processes, other thin-film deposition techniques create much "rougher" interfaces.[17] As such, we have limited the discussion here to diffuse phonon scattering at the interface.

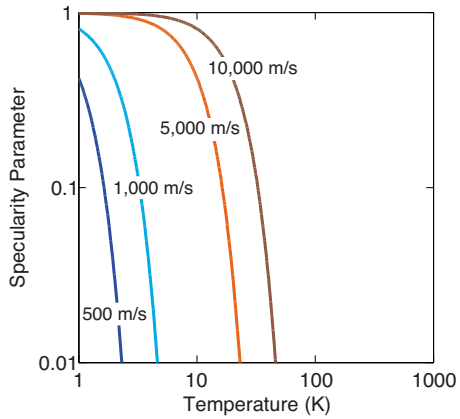

FIG. 1. (Color online) The specularity parameter as a function of temperature plotted for several different group velocities for an assumed interface roughness of 1 nm. The specularity parameter is a measure of the probability a phonon will scatter specularly at an interface. The fastest traveling phonons in Si ($v_{max}=8,192$ m/s) have less than a 1% chance of scattering specularly at 40 K. For lower group velocities, rougher surfaces, or higher temperatures, the probability of phonons scattering specularly is even lower. As such, we have limited the discussion here to diffuse phonon scattering at the interface.

Under the diffuse assumption, the phonon transmissibility from side 1 to side 2 must relate to the phonon transmissibility from side 2 to side 1 via the expression $\zeta^{2\to1}=(1-\zeta^{1\to2})$. Hence, through the application of detailed balance, $q_z^{1\to2}=q_z^{2\to1}$, it is possible to solve for $\zeta^{1\to2}$ explicitly. However, the formulation of the transmission coefficient is largely dependent on the assumptions invoked when applying detailed balance.[10] In the following derivation, it is assumed the type of scattering can be either elastic or inelastic. The purpose of considering both of these cases is twofold. First, it will be shown that these treatments are self-consistent and converge at low temperatures, indicating a minimum temperature at which inelastic processes may start to contribute to interfacial transport. Second, these independent formulations will allow for the construction of upper and lower bounds on the predicted value of thermal boundary resistance. The formulations of the transmission coefficient under these assumptions are discussed in brief below.

A. Elastic scattering at the interface

In the limit of elastic scattering, a phonon in material A on side 1 of the interface can scatter with a phonon in material B on side 2 only if $\omega_{j,1}(k_{j,1})=\omega_{j,2}(k_{j,2})$. As a result, to derive the elastic transmission coefficient, detailed balance should be applied to the phonon flux approaching the interface from both sides on a per frequency basis. Consequently, if a particular phonon frequency does not exist in material A, despite existing in material B, or vice versa, that phonon frequency cannot participate in interfacial transport. Starting in k-space under the assumption of detailed balance and diffuse scattering, the transmission coefficient from side 1 to 2 is given by

$$\zeta^{1\to2}(k_1)=\frac{\Sigma_j\hbar\omega_{j,2}k_{j,2}^2v_{j,2}f_0dk_{j,2}}{\Sigma_j\hbar\omega_{j,2}k_{j,2}^2v_{j,2}f_0dk_{j,2}+\Sigma_j\hbar\omega_{j,1}k_{j,1}^2v_{j,1}f_0dk_{j,1}}. \tag{4}$$

The summations over the different polarizations, j, enforce the assumption of diffuse scattering, thus letting the flux of phonons of one polarization scatter to any other polarization. This presentation of the transmission coefficient, while a function of wavevector, has the restriction that only wave vectors corresponding to the phonon frequency of interest are considered. To make this apparent, the well known relationship between wave vector, frequency, and group velocity, $v(k)\equiv d\omega(k)/dk$, is invoked. As such, Eq. (4) can be rewritten and simplified as

$$\zeta^{1\to2}(\omega)=\frac{\Sigma_j[k_{j,2}(\omega)]^2}{\Sigma_j[k_{j,2}(\omega)]^2+\Sigma_j[k_{j,1}(\omega)]^2}. \tag{5}$$

If the Debye assumption were to be made, Eq. (5) reduces to that derived in the original presentation of the DMM.[5] However, in the original presentation of the DMM, this formulation of the transmission coefficient is only valid up to the highest phonon frequency common to all phonon branches in both materials on sides 1 and 2 of the interface. Due to the combination of both this imposed limit and the Debye assumption, the transmission coefficient is constant for all participating phonon frequencies. For all other phonon frequencies, the transmission coefficient was effectively zero. In this study, under the elastic scattering assumption, $\zeta^{1\to2}$ is defined for all frequencies that exist in both materials A and B on each side of the interface, regardless of how many branches contain that frequency. As described by Duda *et al.*,[10] this ensures that no incident phonon flux approaching the interface is ignored. As a result, the transmission coefficient, even under the Debye assumption, is a function of phonon frequency, as seen in the center column of Fig. 2. These calculations are discussed in more detail within Sec. II B.

B. Inelastic scattering at the interface

At the limit where all elastic and inelastic channels are considered, a phonon in material A on side 1 of the interface can scatter with a phonon in material B on side 2 even if $\omega_{j,1}(k_{j,1})\neq\omega_{j,2}(k_{j,2})$. As a result, all phonons on both sides of the interface can participate in interfacial transport processes. Starting again under the assumption of diffuse scattering, but now applying detailed balance to the total flux at the interface (not per frequency, as in the elastic case), and thus including contributions from all elastic and inelastic channels, the transmission coefficient becomes

$$\zeta^{1\to2}=\frac{\Sigma_j\int_{k_{j,2}}\hbar\omega_{j,2}k_{j,2}^2v_{j,2}f_0dk_{j,2}}{\Sigma_j\int_{k_{j,2}}\hbar\omega_{j,2}k_{j,2}^2v_{j,2}f_0dk_{j,2}+\Sigma_j\int_{k_{j,1}}\hbar\omega_{j,1}k_{j,1}^2v_{j,1}f_0dk_{j,1}}. \tag{6}$$

As before, summations over polarizations, j, enforce the assumption of diffuse scattering. The integrals over the entire Brillouin half-space in both materials A and B indicate that the flux of a phonon of any wave vector or frequency on side 1 can interact with a phonon of any wave vector or frequency on side 2. However, due to this integration, with the integration limits being a function of properties of material A on side 1 and material B on side 2, the inelastic transmission coefficient is different from the elastic transmission coefficient in two ways. First, the transmission coefficient is no longer a function of frequency, as in the limit of elastic scattering, but is rather a single value. Second, the equilibrium distributions do not cancel as they do in the elastic case. As a result, ζ becomes a function of temperature, $\zeta(T)$. It is important to note, for reasons still yet to be discussed, that the T-dependence is related to the assumed equilibrium distribution of the incident phonon flux, and not related to any possible temperature drop at the interface. Again, as with the elastic case, this formulation is discussed in length in other work.[10]

We digress at this point to discuss the implication of Eq. (6), and the DMM formulation in general, on modeling inelastic scattering. Above the Debye temperature, the phonon population is no longer driven quantum mechanically, but classically,[21] which takes a linear dependence on temperature. Therefore, assuming elastic scattering, R_{BD} will be constant at temperatures above the limiting Debye temperature of the two materials since R_{BD} is proportional to the

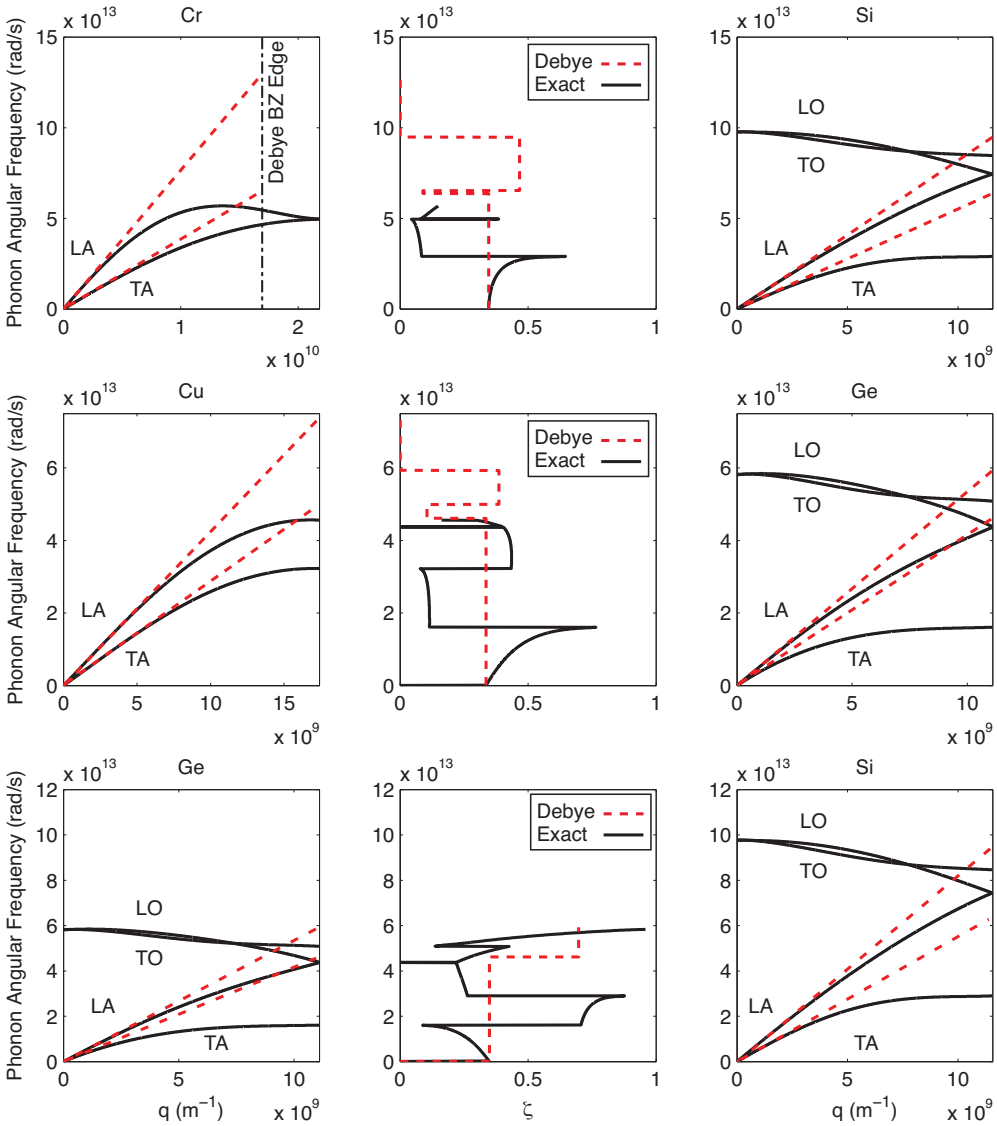

FIG. 2. (Color online) The frequency-dependent elastic transmission coefficients (center column) for the Cr–Si (top), Cu–Ge (middle), and Ge–Si (bottom) interfaces, as well as the dispersion diagrams of the constituent materials. The solid black lines represent the values using the isotropic [100] dispersion, while the dashed red lines represent the values when using the Debye dispersion. In all cases the transverse branches (TA and TO) are doubly degenerate due to the crystallographic symmetry. Regardless of the dispersion relationship, the elastic transmission coefficient (center column) increases when the number of phonon states per wave vector ($\Sigma_j d\omega_j/dk_j$) increases on side 2 or decreases on side 1, and decreases in the opposite cases.

temperature derivative of the phonon population. Following this, R_{BD} will be constant when temperatures are elevated above the Debye temperature of both materials comprising the interface when considering inelastic scattering via Eq. (6). Previous works have shown that inelastic scattering can contribute to R_{BD} both in the regime where neither or only one material is in the classical limit (we will refer to this as the quantum regime)[11,12,22–26] and in the regime where both materials are in the classical limit (referred to as the classical regime).[27–29] Therefore, there are two different regimes where inelastic phonon scattering has shown to play a role in R_{BD}: the classical regime and the quantum regime. As any formulation of R_{BD} based on the DMM, or other models that treat R_{BD} as a derivative of a phonon population, will predict a constant h_{BD} in the classical limit, we focus this work on developing the present formulation to elucidate the role of interfacial phonon scattering in the quantum regime.

C. Application to thermal boundary conductance

The relationship between the phonon flux traversing an interface from side 1 to side 2 and thermal boundary conductance, $h_{BD}=(R_{BD})^{-1}$, can be established through a modified form of Fourier's law and noting that

$$q_z^{1\to 2} = h_{BD}^{1\to 2} T^{1\to 2}, \tag{7}$$

where $T^{1\to 2}$ is the temperature drop across the interface. The main thermophysical processes on which this work is focused are the phonon interfacial scattering processes which are described by the transmission coefficients. We therefore focus our control volume around the fluxes approaching the interface within a MFP. As we are considering only the effects of interfacial processes, and not their relations to the temperature gradient developed in the materials comprising the interface, and since we are only considering completely

diffusive scattering events (i.e., a fully thermalizing black boundary), we will retain our h_{BD} analysis using Eq. (7) based on the so-called equilibrium flux in Eq. (1). To account for phonon scattering in the materials on either side of the interface and therefore the existence of a temperature gradient (i.e., to account for a large control volume which includes anharmonic processes in the materials adjacent to the interface), Eq. (1) should be reformulated using a diffusion-transmission boundary condition.[30,31] This formulation has been derived in detail by Landry and McGaughey.[29] However, regardless of formulation, the transmission coefficients at the interface must be determined, and in the diffusive regime these are described by the detailed balance formulation described previously[10] With this in mind, h_{BD} is given by

$$h_{BD}^{1\to 2} = \frac{1}{8\pi^2}\sum_j \int_{k_{j,1}} \hbar\omega_{j,1}(k_{j,1})k_{j,1}^2\zeta^{1\to 2}|v_{j,1}(k_{j,1})|\frac{\partial f_0}{\partial T}dk_{j,1}. \tag{8}$$

It is important to remember that, for all intents and purposes, the transmission coefficient has already been formulated at this point in the derivation of the DMM. As a result, it is critical that any restrictions or allowances regarding the range of participating phonons established during the application of detailed balance and the formulation of the transmission coefficient must be upheld here as well.

III. RESULTS

In this section three interfaces of interest are examined: Cr–Si, Cu–Ge, and Ge–Si. The DMM will be applied to each of these interfaces in order (i) to compare the Debye and isotropic [100] phonon dispersion relationships, (ii) to establish the upper and lower limits of h_{BD} under the assumptions of inelastic and elastic scattering, and (iii) to evaluate the contribution of optical phonons to interfacial thermal transport processes. Lastly, the accuracy of an assumed isotropic dispersion based on the exact phonon dispersion in either the [100] or [111] crystallographic directions will be evaluated by comparing predicted values of h_{BD} at the Cu–Ge interface for these scenarios to those values predicted through the use of an exact three-dimensional dispersion.[15]

A. Comparison of the Debye and isotropic [100] dispersion relationships

In order to compare the Debye and isotropic dispersion relationships, exact phonon dispersion relationships of Cr,[32] Cu,[33] Ge, and Si (Ref. 34) were taken from the literature. The dispersion relationships describing each phonon branch in the [100] direction were fit with fourth-order polynomials, establishing both phonon frequency and group velocity (given by $d\omega/dk$) for each branch as fourth and third order polynomial functions of k, respectively.[35] The Debye dispersion relationships were formulated by taking the linear coefficients of the fourth order polynomials describing the acoustic phonon branches of each material and extrapolating lines tangential to the dispersion curves at the zone center to the Debye BZ (DBZ) edge. That is, if a phonon branch in the isotropic [100] dispersion is given by $\omega(k)=Ak^4+Bk^3+Ck^2+Dk$, where A, B, C, and D, are the polynomial coefficients, the corresponding Debye dispersion is given by $\omega(k)=Dk$ and $v_D=D$. Using these values, D was within 5% of the sound velocities of the materials of interest, suggesting this method of determining Debye dispersion should agree with the traditional method (using experimentally determined sound velocities and densities).

Figure 2 shows the frequency-dependent elastic transmission coefficients (center column) for the Cr–Si (top), Cu–Ge (middle), and Ge–Si (bottom) interfaces, as well as the dispersion diagrams of the constituent materials. The solid black lines represent the values using the isotropic [100] dispersion, while the dashed red lines represent the values when using the Debye dispersion. In all cases the transverse branches (transverse acoustic, TA, and transverse optical, TO) are doubly degenerate due to the crystallographic symmetry of cubic crystals in the [100] direction. The maximum Debye wave vector, or DBZ edge, for each material is given by $k_D=\omega_D/v_D$, where $\omega_D=v_D(6\pi N)^{1/3}$ and N is the lattice point density. In the cases of Cu, Ge, and Si, the respective DBZ edges are within 2% of the real BZ edges in the [100] direction. However, in Cr, the DBZ edge is at $k_D=1.70\times10^{10}$ m^{-1}, while the BZ edge in the [100] direction is at $k=2.18\times10^{10}$ m^{-1}. Due to the significant difference between the Debye and real zone edges in Cr, the DBZ edge has been illustrated in the dispersion diagram of Cr in Fig. 2 (top left). For the other materials considered, the minor differences between the DBZ and the BZ edges are omitted for the sake of clarity.

In all cases, the Debye dispersion greatly over-predicts the maximum phonon frequency of each branch in the [100] direction. This over-prediction is particularly noticeable in Cr and Cu, where there are no high-frequency optical phonons. The discontinuities in the elastic transmission coefficient, (ζ, middle column) can be mapped back to an appearance or extinction of a phonon branch on either side of the interface. A "positive" discontinuity (where ζ increases) occurs when a branch on side 1 disappears or a branch on side 2 appears, while a "negative" discontinuity occurs in the opposite cases. This is true for both the Debye and isotropic dispersion relationships. Similarly, with the isotropic [100] dispersion relationships, if a particular branch is leveling off with increasing phonon frequency on side 2 (right column) while the slopes of the branches on side 1 (left column) remain constant, the transmission coefficient increases; this is the behavior described by Eq. (4). On the other hand, if a particular branch is leveling off on side 1 while the slopes of the branches on side 1 remain constant, the transmission coefficient decreases. In other words, the elastic transmission coefficient increases when the number of phonon states per wave vector ($\Sigma_j d\omega_j/dk_j$) increases on side 2 or decreases on side 1, and decreases in the opposite cases.

Figure 3 shows the ratio of the DMM predicted values of h_{BD} using the Debye and isotropic [100] dispersion relationships ($h_{BD}^{Debye}/h_{BD}^{[100]}$) as a function of temperature for Cr–Si, Cu–Ge, and Ge–Si interfaces. Regardless of the assumed type of scattering, this ratio is greater or equal to one for all

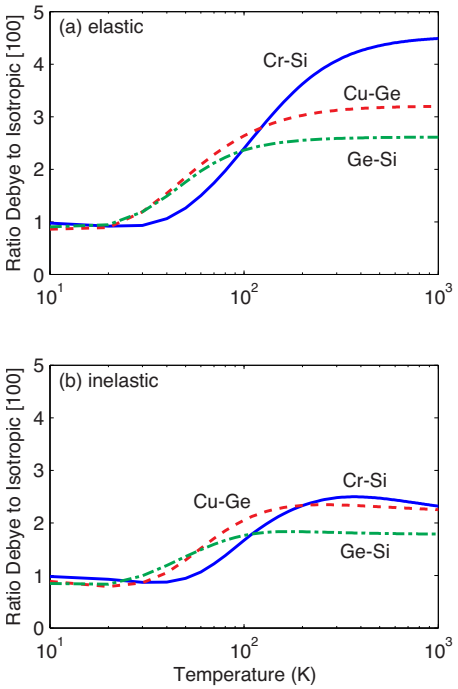

FIG. 3. (Color online) The ratio of the predicted value of h_{BD} using the Debye and isotropic [100] dispersion relationships as a function of temperature for the Cr–Si, Cu–Ge, and Ge–Si interfaces assuming (a) elastic and (b) inelastic scattering at the interface. The over-prediction is not as great for Cu–Ge and Ge–Si interfaces, where the Debye model's over-predictions of the acoustic phonon frequencies and velocities are coincidentally compensated for (to an extent) by its lack of consideration of the optical phonons. That is, since the Debye model ignores optical phonons and the isotropic model includes them, the additional interfacial flux due to the optical phonons in the isotropic model offsets the Debye models over-prediction of the acoustic phonons.

interfaces over the entire temperature range. Ultimately, the transmission coefficient alone cannot be responsible for this over-prediction as, by form, it is confined to a value between 0 and 1. Thus, the over-prediction of the Debye model relative to the isotropic [100] model is due to the Debye model's tendency to over-predict the phonon flux approaching the interface (the Debye model incorrectly predicts the existence of high-velocity, high energy-phonons near the zone edge). This over-prediction is particularly substantial in the case of the Cr–Si interface, where the maximum phonon frequency is not at the BZ edge. However, this over-prediction is not as great for Cu–Ge and Ge–Si interfaces, where the Debye model's over-predictions of the acoustic phonon frequencies and velocities are coincidentally compensated for (to an extent) by its lack of consideration of the optical phonons. That is, since the Debye model ignores optical phonons and the isotropic [100] model includes them, the additional interfacial flux considered by the isotropic model offsets the Debye models over-prediction of the acoustic phonons.

B. Assumptions of elastic and inelastic scattering at the interface

When comparing Figs. 3(a) and 3(b) it is apparent that the ratio between predicted values of h_{BD} using the Debye and isotropic [100] dispersion relationships ($h_{BD}^{Debye}/h_{BD}^{[100]}$) is greater in the elastic case than in the inelastic case. This can

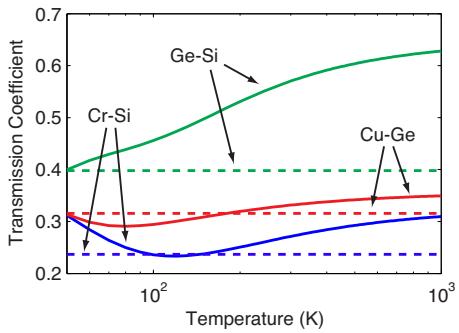

FIG. 4. (Color online) A comparison of the elastic and inelastic transmission coefficients for the three interfaces of Cr–Si, Cu–Ge, and Ge–Si interfaces. The elastic transmission coefficients (dashed lines) were calculated by averaging the frequency dependent values shown in Fig. 2, and as discussed, are temperature independent. Inelastic coefficients (solid lines) generally increase with increasing temperature.

be explained in the following way. In the elastic case, participation in interfacial transport processes is restricted to primarily acoustic phonons. This is especially true in the case of the Cr–Si interface, where the optical phonons in Si are not accessible to the acoustic phonons in Cr (under the assumption of elastic scattering). In the inelastic case, all acoustic and optical phonons can participate. As mentioned above, the ratio between the Debye model and the isotropic [100] model is smaller for those interfaces where optical phonons are present. Likewise, by enabling the optical branches to participate in full, once again the Debye model's over-predictions of the acoustic phonon frequencies and velocities are compensated for by its lack of consideration of the optical phonons. Again, the Debye model was not intended to capture the effects of the optical phonons, and this compensation is merely coincidental.

Figure 4 shows a comparison of the elastic and inelastic transmission coefficients for Cr–Si, Cu–Ge, and Ge–Si interfaces. The elastic transmission coefficients (dashed lines) were calculated by averaging the frequency dependent values shown in the center column of Fig. 2, and, as discussed, are temperature independent. Inelastic transmission coefficients (solid lines) generally increase with increasing temperature. Ultimately, the slope of the inelastic curves, $\partial\zeta/\partial T$, is positive when the occupied density of states on side 2 increases relative to the occupied density of states on side 1 with increasing temperature. This can be expressed mathematically by recognizing the temperature derivative of Eq. (6) goes as

$$\frac{\partial \zeta}{\partial T} \propto \frac{\partial}{\partial T}\left(\frac{\int_{k_2} f_0}{\int_{k_2} f_0 + \int_{k_1} f_0}\right). \tag{9}$$

At the Cu–Ge interface, the inelastic transmission coefficient decreases as temperature increases from 50 to 80 K. Thus, it can be said that, within this temperature range, the occupied density of states in Cu is increasing faster with temperature than it is in Ge.

The ratios of the inelastic and elastic predictions of h_{BD} using isotropic [100] dispersion ($h_{BD}^{inel}/h_{BD}^{el}$) for Cr–Si, Cu–Ge, and Ge–Si interfaces are presented in Fig. 5. In prior inelastic treatments of the DMM, Debye dispersion relationships were used to describe the materials comprising the in-

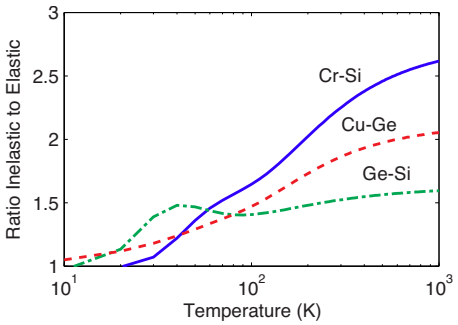

FIG. 5. (Color online) Ratio of the inelastic and elastic predictions of h_{BD} using isotropic [100] dispersion. As expected, the temperature dependence of the Bose-Einstein distribution function ensures that the ratio $h_{BD}^{inel}/h_{BD}^{el}$ generally increases with increasing temperature. Additionally, this ratio is larger for interfaces between materials with a limited range of phonon frequency overlap (i.e., Cr–Si).

terface. As a result, the shapes of these curves were the same regardless of the interface and only the magnitude of the presented ratio differed.[36] Here, however, the shapes vary significantly from interface to interface due to the nonlinear behavior of the phonon dispersion. Still, as previously shown with the Debye model, the higher the temperature, the greater the inelastic to elastic ratio. Additionally, for interfaces characterized by large vibrational mismatch (where the overlap between each material's phonon density of states is small), inelastic scattering can play a larger role at elevated temperatures.[36]

C. Contribution of optical phonons to interfacial transport

Through the use of isotropic [100] dispersion relationships, the relative contribution of optical phonons can be determined explicitly. Figure 6 illustrates the contribution of optical phonons to the DMM predicted values of h_{BD} under the (a) elastic and (b) inelastic scattering assumptions. Again, at the Cr–Si interface, under the assumption of elastic phonon scattering, the optical phonons in Si are inaccessible to the acoustic phonons in Cr. As a result, optical phonons under this scattering assumption do not contribute to interfacial transport at the Cr–Si interface. However, optical phonons do participate in elastic phonon processes at both Cu–Ge and Ge–Si interfaces. At the Ge–Si interface in particular, these contributions can be significant, exceeding 40% of the total predicted value of h_{BD}. That is, $h_{BD}^{optical}/(h_{BD}^{acoustic}+h_{BD}^{optical}) > 40\%$. Under the assumption of inelastic scattering at the interface, optical phonons play a role at all three interfaces studied. Surprisingly, the contribution of optical phonons to interfacial transport at these interfaces is significant even at relatively low temperatures, i.e., $T<100$ K. The contribution of optical phonons in interfacial transport processes is explored further elsewhere.[19]

D. Comparison of isotropic one-dimensional (1D) and exact three-dimensional (3D) dispersion relationships

Throughout this study we've assumed that it is fair to describe the phonon dispersion of a cubic crystal with an

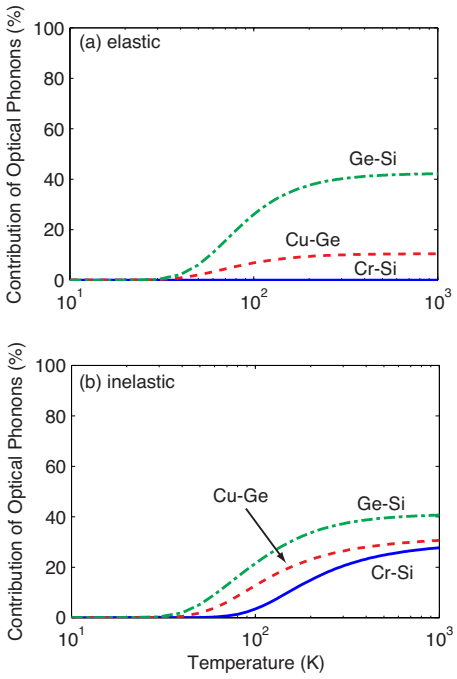

FIG. 6. (Color online) The contribution of optical phonons to the predicted value of h_{BD} using the isotropic [100] phonon dispersion under the assumptions of (a) elastic and (b) inelastic scattering. There is no optical phonon contribution at Cr–Si interfaces under the elastic scattering assumption, whereas the optical phonons contribute in excess of 40% at 300 K for the Ge–Si interface.

isotropic dispersion relationship taken from the exact phonon dispersion in the [100] crystallographic direction. In an attempt to evaluate the accuracy of the assumption, the predicted value of h_{BD} for a Cu–Ge interface using this isotropic [100] dispersion relationship is compared to predictions using an isotropic [111] dispersion relationship and the data from Reddy *et al.*, (where exact 3D phonon dispersions are first calculated via a BKM).[15] We use this 3D exact-phonon model as a means of comparison rather than experimental data for two reasons. First, this exact-dispersion model represents the most thorough and computationally expensive means of predicting h_{BD} as a function of the vibrational properties of the materials comprising the interface alone. Second, as discussed at length in the introduction, many additional aspects of the interface can influence h_{BD}. Without intimate knowledge of the interfacial conditions corresponding to experimentally measured values, assessing the accuracy of this model would be difficult.

The aforementioned exact-phonon model[15] study did not take into consideration the role of optical phonons. Consequently, the optical phonons have been intentionally left out of the calculations in this section. Predictions of h_{BD} using Debye dispersions, isotropic [100] and [111] dispersions, and exact 3D phonon dispersions are compared in Fig. 7. As seen in the figure, for a majority of the temperature range the isotropic [100] and [111] dispersions bound the values predicted using the exact three-dimensional phonon dispersion. The reason for the slight difference in the initial rise of the data cannot be known without further details regarding the formulation of Reddy *et al.*, especially with regard to the manner in which detailed balance was applied. The chosen

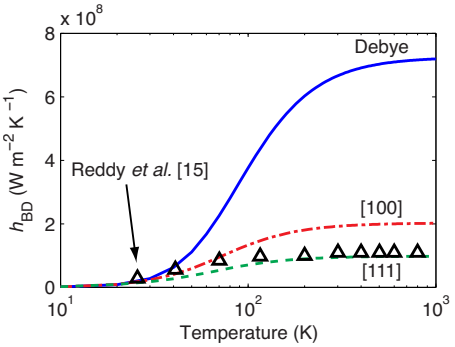

FIG. 7. (Color online) Comparison of the elastic-isotropic formulation of the DMM presented here to the exact phonon dispersion presentation of Reddy *et al.* (Ref. 15). To examine the influence of chosen crystallographic direction on the accuracy of the present model, phonon dispersions in two directions of high symmetry ([100] and [111]) were implemented for the Cu–Ge interface. In order to compare these cases directly, optical phonons were intentionally ignored. As seen, for a majority of the temperature range, the two crystallographic directions bound the values predicted using the 3D phonon dispersion. The source of the slight difference in the initial rise of the data points cannot be known without further details regarding the formulation of Reddy *et al.* However, it is reasonable that this difference could be the result of a different formulation of detailed balance (Ref. 10).

crystallographic direction does, in fact, introduce some variability with regards to the predicted value, although the 1D and 3D exact-dispersion values are grouped within a factor of 2, whereas the Debye model is off by a factor of 7 at elevated temperatures. Implementing the isotropic approach then, while no doubt reducing the final accuracy of the model, allows for significant improvements over the traditional DMM without the need for the computational expense and expertise needed in a full 3D model.

IV. CONCLUSION

The role of phonon dispersion in the prediction of thermal boundary conductance via the diffuse mismatch model has been examined. All calculations were carried out under both the assumptions of elastic and inelastic phonon scattering at the interface. It was shown that the Debye dispersions most frequently used in the DMM lead to an over-prediction of the phonon flux approaching the interface, and hence, an over-prediction of h_{BD} at Cr–Si, Cu–Ge, and Ge–Si interfaces. The role of optical phonons in interfacial transport processes was briefly discussed, and it was shown that their contribution to thermal transport across an interface between Ge and Si can be in excess of 40% of total transport. It is reasonable to assume this value could be much greater for interfaces comprised of materials with more optical phonon branches. Additionally, if the contribution of optical phonons was large enough, the over-prediction associated with the Debye dispersion could be mitigated entirely. Lastly, the accuracy of the assumed isotropic [100] dispersions was evaluated by comparing the predicted value of h_{BD} using these dispersion relationships with predictions using isotropic [111] dispersion relationships and exact 3D phonon dispersion relationships for an interface between Cu and Ge. It was seen that, using [100], [111], and exact three-dimension phonon dispersion, the predicted values were in general agreement with each other and displayed the same temperature dependence.

ACKNOWLEDGMENTS

The authors at U.Va. would like to acknowledge the financial support of the Air Force Office of Scientific Research (Grant No. FA9550-09-1-0245). J.C.D. is greatly appreciative for financial support from the National Science Foundation through the Graduate Research Fellowship Program. P.E.H. is grateful for funding from the LDRD program office through the Sandia National Laboratories Harry S. Truman Fellowship. Sandia National Laboratories is a multiprogram laboratory operated by Sandia Corporation, a wholly owned subsidiary of Lockheed-Martin Co., for the United States Department of Energy's National Nuclear Security Administration under Contract No. DE-AC04-94AL85000.

[1]G. Chen, *Nanoscale Energy Transport and Conversion: A Parallel Treatment of Electrons, Molecules, Phonons, and Photons* (Oxford University Press, New York, 2005).
[2]S. M. Sze and K. K. Ng, *Physics of Semiconductor Devices*, 3rd ed. (Wiley, New York, 2007).
[3]L. W. da Silva and M. Kaviany, Int. J. Heat Mass Transfer **47**, 2417 (2004).
[4]W. A. Little, Can. J. Phys. **37**, 334 (1959).
[5]E. T. Swartz and R. O. Pohl, Rev. Mod. Phys. **61**, 605 (1989).
[6]R. J. Stoner and H. J. Maris, Phys. Rev. B **48**, 16373 (1993).
[7]R. J. Stevens, A. N. Smith, and P. M. Norris, J. Heat Transfer **127**, 315 (2005).
[8]T. Beechem, S. Graham, P. Hopkins, and P. Norris, Appl. Phys. Lett. **90**, 054104 (2007).
[9]T. Beechem and P. E. Hopkins, J. Appl. Phys. **106**, 124301 (2009).
[10]J. C. Duda, P. E. Hopkins, J. L. Smoyer, M. L. Bauer, T. E. English, C. B. Saltonstall, and P. M. Norris, Nanoscale Microscale Thermophys. Eng. **14**, 21 (2010).
[11]P. E. Hopkins and P. M. Norris, Nanoscale Microscale Thermophys. Eng. **11**, 247 (2007).
[12]P. E. Hopkins, J. Appl. Phys. **106**, 013528 (2009).
[13]J. C. Duda, J. L. Smoyer, P. M. Norris, and P. E. Hopkins, Appl. Phys. Lett. **95**, 031912 (2009).
[14]P. E. Phelan, J. Heat Transfer **120**, 38 (1998).
[15]P. Reddy, K. Castelino, and A. Majumdar, Appl. Phys. Lett. **87**, 211908 (2005).
[16]P. E. Hopkins and P. M. Norris, Appl. Phys. Lett. **89**, 131909 (2006).
[17]P. E. Hopkins, P. M. Norris, R. J. Stevens, T. E. Beechem, and S. Graham, J. Heat Transfer **130**, 062402 (2008).
[18]J. D. Chung, A. J. H. McGaughey, and M. Kaviany, J. Heat Transfer **126**, 376 (2004).
[19]T. E. Beechem, J. C. Duda, P. E. Hopkins, and P. M. Norris (unpublished).
[20]P. M. Norris and P. E. Hopkins, J. Heat Transfer **131**, 043207 (2009).
[21]C. Kittel, *Introduction to Solid State Physics*, 8th ed. (Wiley, Hoboken, New Jersey, 2005).
[22]P. E. Hopkins, R. N. Salaway, R. J. Stevens, and P. M. Norris, Int. J. Thermophys. **28**, 947 (2007).
[23]P. E. Hopkins, P. M. Norris, and R. J. Stevens, J. Heat Transfer **130**, 022401 (2008).
[24]H.-K. Lyeo and D. G. Cahill, Phys. Rev. B **73**, 144301 (2006).
[25]C. Dames and G. Chen, J. Appl. Phys. **95**, 682 (2004).
[26]G. Chen, Phys. Rev. B **57**, 14958 (1998).
[27]Y. Chen, D. Li, J. Yang, Y. Wu, J. R. Lukes, and A. Majumdar, Physica B **349**, 270 (2004).
[28]R. J. Stevens, L. V. Zhigilei, and P. M. Norris, Int. J. Heat Mass Transfer **50**, 3977 (2007).
[29]E. S. Landry and A. J. H. McGaughey, Phys. Rev. B **80**, 165304 (2009).

[30]G. Chen, Appl. Phys. Lett. **82**, 991 (2003).
[31]W. G. Vincenti and C. H. Kruger, *Introduction to Physical Gas Dynamics* (Krieger, Malabar, FL, 2002).
[32]R. C. Rai and M. P. Hemkar, J. Phys. F: Met. Phys. **8**, 45 (1978).
[33]S. K. Sinha, Phys. Rev. **143**, 422 (1966).
[34]W. Weber, Phys. Rev. B **15**, 4789 (1977).
[35]E. Pop, S. Sinha, and K. E. Goodson, Proc. IEEE **94**, 1587 (2006).
[36]P. E. Hopkins and P. M. Norris, J. Heat Transfer **131**, 022402 (2009).